ELSEVIER

Journal of Nuclear Materials 302 (2002) 143–155

journal of nuclear materials

www.elsevier.com/locate/jnucmat

Microstructure modelling of ferritic alloys under high flux 1 MeV electron irradiations

A. Hardouin Duparc [a], C. Moingeon [a], N. Smetniansky-de-Grande [b], A. Barbu [a,*]

[a] *Laboratoire de Solides Irradiés, CEA-CNRS-EcolePolytechnique, 91128 Palaiseau cedex, France*
[b] *Departamento de Materiales, CNEA, Avda. del Libertador 8250, 1429 Buenos Aires, Argentina*

Received 1 July 2001; accepted 21 January 2002

Abstract

The point-defect clustering is an important component of the hardening of low copper content pressure vessel steels. This study reports the first steps of a project devoted to the modelling of the nucleation and growth of point-defect clusters in ferritic alloys under irradiation at large fluence. A cluster-dynamics modelling based on rate equations giving the evolution of the population of interstitial loops up to some 0.1 μm and of vacancy clusters is developed. It is applied to two alloys FeCu (0.13 wt%) and FeMn(1.5 wt%)Ni(0.8 wt%)Cu(0.13 wt%)P(0.01 wt%) the composition of which is close to the one of pressure vessel steels and to non-alloyed Fe for comparison. The model was calibrated by carrying out 1 MeV irradiations in a high voltage microscope on these three materials and by using the results of experiments and atomic simulations reported in the literature. It is shown that the presence of copper in iron stabilises the interstitial clusters and more important that the parameters relative to the interstitials in the complex alloys are totally different from those for iron: the migration energy must be increased from 0.3 to 1 eV and the binding energy of di-interstitials must be decrease from 0.9 to 0.2 eV. © 2002 Published by Elsevier Science B.V.

PACS: 61.82.Bg; 61.80.Fe; 60.00.Hg

1. Introduction

The radiation hardening of metallic alloys under irradiation is known to be due to radiation-induced features such as point-defect clusters or precipitates which are generally large enough to be observed by transmission electron microscopy (TEM).

In the case of pressure vessel steels, the combination of material and external parameters are such that the microstructural features induced by irradiation resulting in hardening and associated embrittlement are too small to be observed by TEM [1]. Till now, in very low copper content steels ([Cu] $\leqslant$ 0.1%), no copper precipitates have been experimentally observed except for diffuse three-dimensional segregation. Their radius is around 2 nm and they contain mainly manganese, nickel and silicon atoms that are known to be soluble in iron and only few copper atoms [2].

Concerning the point-defect clusters, very small three-dimensional vacancy clusters (three to four vacancies) have been seen experimentally by positron annihilation spectroscopy in irradiated steels at $T \leqslant 150$ °C but likely not at in service temperature [3]. Furthermore, indirect evidences show that small point-defect clusters are induced by irradiation and that they are not only nucleated in the core of the cascades but also by the random encounter of self-interstitial atoms (SIA): a hardening of 30 $Hv_{0.05}$ (Vickers test under a load of 50 g) is obtained in an Fe(0.11 at.%)Cu alloy irradiated with 2.5 MeV electrons up to 1.4×10^{-3} dpa at 290 °C [4] and an hardening of 26 $Hv_{0.5}$ in an Fe(0.08 at.%)Cu alloy irradiated with 2.5 MeV electrons up to 8.7×10^{-4} dpa

* Corresponding author. Tel.: +33-1 69 33 44 98; fax: +33-1 69 33 30 22.
E-mail address: alain.barbu@poly.polytechnique.fr (A. Barbu).

0022-3115/02/$ - see front matter © 2002 Published by Elsevier Science B.V.
PII: S0022-3115(02)00776-6

at 300 °C [5], when no solute segregation is observed by tomographic atom probe [2]. Irradiation with neutrons in the Osiris experimental reactor up to 8×10^{-2} dpa at 290 °C gave $Hv_{0.05} = 73$ in the first model alloy [6] and $Hv_{0.5} = 53$ in the second [7]. So, taking into account the fact that the fluence reached, expressed in dpa, is smaller for the electron than for the neutron irradiations, we can conclude that the mode of production of the elementary damage (isolated point defects or displacement cascades) has surprisingly not a strong effect on the hardening. As shown recently, this behaviour is also observed in pressure vessel steels at the operating temperature [8] as well as at 60 °C [9].

To increase the lifetime of the nuclear plant, it is of prime importance to be able to predict the embrittlement. Empirical formulae built for the case of samples irradiated under accelerated conditions are used for this purpose. However, it seems important to validate these extrapolations by taking into account the physical phenomena underlying the degradation of the mechanical properties under operating condition. In the case of low copper pressure vessel steels, point-defect clusters are an important cause of hardening. Then, modelling the nucleation and growth of point-defect clusters is necessary.

The best way to do it would be to carry out atomic simulation up to the end of life of the vessel. Despite the important increase of the capability of computers it remains nowadays out of reach especially if we consider the size of a representative volume. Then, using cluster-dynamics modelling based on rate equations is still the only option. Indeed, they are based on important simplifications and need the knowledge of sets of parameters characteristic of the material. These parameters can be obtained by atomic simulations or experimentally. It is worth noticing that too often, pure iron parameters are used. We will show that they are not appropriate for alloys with a composition close to that of the pressure vessel steels.

The purpose of this paper is to present the beginning of a project which consists in developing and using a cluster-dynamics modelling in parallel with experimental studies on ferritic alloys. It consists of:

1. Modelling SIA and vacancy clustering using a cluster-dynamics modelling (mean field model or rate equations modelling).
2. Studying the nucleation and growth of interstitial loops in model alloys under 1 MeV irradiation in a high voltage electron microscope (HVEM) i.e. under irradiation condition where the point-defect clusters are observable by TEM.
3. Finding a set of parameters of the model giving an acceptable fit of the experimental results obtained in step 2.
4. Calculating the distribution of clusters under the low dose rate electron irradiation condition, corresponding to the one obtained using a Van de Graaff accelerator, and testing if the clusters are actually two small to be visible (or eventually have a too low number density) and if the deduced hardening is in agreement with the measured one [4].
5. Repeating steps 2–4 but under irradiation conditions where displacement cascades are produced (ion irradiations).

We will here consider only the steps 1–3 and that only SIA and vacancies are mobile. The effect of the mobility of the clusters, will be discussed in a companion paper.

We guess that starting this study with electron irradiations, i.e. under conditions where the primary damage is simple (isolated point defects) is of primary importance to test the model: any modelling of the evolution of steels or any other material under neutron irradiation should at least be able to reproduce this simple situation.

2. The model

Cluster-dynamics modelling were used very soon to describe the point-defect clustering. They are all based on the most general equation [10]

$$\frac{\mathrm{d}C_j}{\mathrm{d}t} = G_j + \sum_k w(k,j)C_k - \sum_k w(j,k)C_j - L_j, \tag{1}$$

where C_j is the concentration of clusters of type j, $w(k,j)$ the transition rate per unit concentration of a cluster of type k to a cluster of type j, G_j the production rate of cluster of type j by collision of the irradiating particles with the material and L_j the loss rate of cluster of type j on all points defect sinks but point-defect clusters.

2.1. Basic equations

Assuming that only SIA and vacancies are mobile, (1) may be rewritten as follows:

$$\left.\begin{aligned}\frac{\mathrm{d}C_{ni}}{\mathrm{d}t} &= \left(\beta^{\mathrm{i}}_{(n-1)\mathrm{i}}C_{1\mathrm{i}}\right)C_{(n-1)\mathrm{i}} + \left(\beta^{\mathrm{v}}_{(n+1)\mathrm{i}}C_{1\mathrm{v}} + \alpha^{\mathrm{i}}_{(n+1)\mathrm{i}}\right)C_{(n+1)\mathrm{i}} \\ &\quad - \left(\alpha^{\mathrm{i}}_{n\mathrm{i}} + \beta^{\mathrm{v}}_{n\mathrm{i}}C_{1\mathrm{v}} + \beta^{\mathrm{i}}_{n\mathrm{i}}C_{1\mathrm{i}}\right)C_{n\mathrm{i}}, \\ \frac{\mathrm{d}C_{n\mathrm{v}}}{\mathrm{d}t} &= \beta^{\mathrm{v}}_{(n-1)\mathrm{v}}C_{1\mathrm{v}}C_{(n-1)\mathrm{v}} + \left(\beta^{\mathrm{i}}_{(n+1)\mathrm{v}}C_{1\mathrm{i}} + \alpha^{\mathrm{v}}_{(n+1)\mathrm{v}}\right)C_{(n+1)\mathrm{v}} \\ &\quad - \left(\beta^{\mathrm{v}}_{n\mathrm{v}}C_{1\mathrm{v}} + \beta^{\mathrm{i}}_{n\mathrm{v}}C_{1\mathrm{i}} + \alpha^{\mathrm{v}}_{n\mathrm{v}}\right)C_{n\mathrm{v}}.\end{aligned}\right\} \tag{2}$$

Here $C_{n\theta}$ is the concentration (number per unit volume) of clusters containing n point defect (size n) of type θ ($\theta = \mathrm{i}$ for interstitial and v for vacancy). $\beta^{\theta'}_{n\theta}C_{1\theta'}$ is the rate of capture of a point defect of type θ' by a cluster of type θ and size n. $\alpha^{\theta'}_{n\theta}$ is the rate of emission of a point defect of type θ' by a cluster of type θ and size n. In (2) we have considered that a cluster of type θ can only emit a point defect of the same type.

In the case of one and two interstitials and one and two vacancies the equations are different

$$\left.\begin{aligned}
\frac{dC_{1i}}{dt} &= G_{1i} - R_{iv}C_{1i}C_{1v} - K_{1i}C_{1i} - 4\beta^{i}_{1i}C_{1i}C_{1i} + 4\alpha^{i}_{2i}C_{2i} \\
&\quad + \beta^{v}_{2i}C_{1v}C_{2i} - C_{1i}\sum_{n=2}\beta^{i}_{ni}C_{ni} + \sum_{n=3}\alpha^{i}_{ni}C_{ni} \\
&\quad - C_{1i}\sum_{n=2}\beta^{i}_{nv}C_{nv}, \\
\frac{dC_{2i}}{dt} &= 2\beta^{i}_{1i}C^{2}_{1i} - 2\alpha^{i}_{2i}C_{2i} - \beta^{i}_{2i}C_{1i}C_{2i} + \alpha^{i}_{3i}C_{3i} - \beta^{v}_{2i}C_{1v}C_{2i} \\
&\quad + \beta^{v}_{3i}C_{1v}C_{3i}, \\
\frac{dC_{1v}}{dt} &= G_{1v} - R_{iv}C_{1i}C_{1v} - K_{1v}\left(C_{1v} - C^{e}_{v}\right) - 4\beta^{v}_{1v}C_{1v}C_{1v} \\
&\quad + 4\alpha^{v}_{2v}C_{2v} + \beta^{i}_{2v}C_{1i}C_{2v} - C_{1v}\sum_{n=2}\beta^{v}_{nv}C_{nv} \\
&\quad + \sum_{n=3}\alpha^{v}_{nv}C_{nv} - C_{1v}\sum_{n=2}\beta^{v}_{ni}C_{ni}, \\
\frac{dC_{2v}}{dt} &= 2\beta^{v}_{1v}C^{2}_{1v} - 2\alpha^{v}_{2v}C_{2v} - \beta^{v}_{2v}C_{1v}C_{2v} + \alpha^{v}_{3v}C_{3v} \\
&\quad - \beta^{i}_{2v}C_{1i}C_{2v} + \beta^{i}_{3v}C_{1i}C_{3v},
\end{aligned}\right\} \tag{3}$$

where R_{iv} is the recombination rate and K_{1i} (respectively K_{1v} the elimination rate of interstitials (respectively vacancies) on fixed sinks as surfaces and dislocations.

The evolution of the cluster size is then obtained through the numerical resolution of a system of $N_i + N_v$ differential equations, where N_i and N_v are respectively the maximum size of interstitial and vacancy clusters. With the current capability of computers and with the constraint of a maximum computation time of some minutes, $N_i + N_v$ cannot be larger than a few hundred. In order to extend this limit which remains too low, the discrete equation is transformed into a continuous Fokker–Plank type equation which describes the evolution of the density of concentration $C(x,t)$ where x is the number of interstitials (respectively vacancies) in the cluster. They have the same form for interstitial and for vacancy cluster. We have [10]

$$\frac{dC_i(x,t)}{dt} = -\frac{\partial}{\partial x}\left[f_i(x)C_i(x,t)\right] + \frac{\partial^2}{\partial x^2}\left[d_i(x)C_i(x,t)\right] \tag{4a}$$

with for $\theta = v$

$$\begin{aligned}
d_v(x) &= \tfrac{1}{2}\left[\beta^{v}_{xv}C_{1v} + \beta^{i}_{xv}C_{1i} + \alpha^{v}_{xv}\right], \\
f_v(x) &= \beta^{v}_{xv}C_{1v} - \beta^{i}_{xv}C_{1i} - \alpha^{v}_{xv}
\end{aligned} \tag{4b}$$

and for $\theta = i$

$$\begin{aligned}
d_i(x) &= \tfrac{1}{2}\left[\beta^{i}_{xi}C_{1i} + \beta^{v}_{xi}C_{1v} + \alpha^{i}_{xi} + \alpha^{v}_{xi}\right], \\
f_i(x) &= \beta^{i}_{xi}C_{1i} - \beta^{v}_{xi}C_{1v} - \alpha^{i}_{xi} + \alpha^{v}_{xi}.
\end{aligned} \tag{4c}$$

It is worth noticing that a term α^{v}_{xi} describing the emission of vacancies from interstitial clusters has been added because for large clusters this term is no more negligible at high temperature. The term α^{i}_{xi} has been left even if it is usually negligible for large interstitial clusters. In fact, with the material and external parameters effectively used, only α^{v}_{xv} and α^{i}_{xi} for very small interstitial clusters are important.

These equations are then discretised in the x space in such way that the increment of Δx between two successive points in the x space increases when x increases. To minimise stability problems, a new variable, inspired by the transformation proposed by Gonhiem and Sharafat [11] is introduced. To avoid any continuity problem between the discrete and continuous equations, the first Δx is set equal to one. This new variable u satisfies the relation

$$u_{k\theta} = \ln\left[(C_{x\theta} - 1)(x_{k\theta} - N_\theta) + 1\right]; \quad \theta = i, v, \tag{5}$$

where $C_{x\theta}$ is a constant greater than unity which drives the increase of Δx with x.

The set of ordinary differential equations is solved numerically using the lsoda package based on a predictor corrector method [12].

2.2. Rate coefficients

The whole physic of this model is contained in production rates and in the rates of capture and emission of point defects by clusters, dislocations, surfaces and grain boundaries.

In order to simplify we will assume that for all but for very small clusters, interstitial and vacancy clusters are two-dimensional clusters (dislocation loops) and we will take into account the multiple sink corrections only for surfaces (thin foil case) or grain boundaries (bulk case).

2.2.1. Production rates of point defects

It is very simple to calculate them in the case of electron irradiations compared to the case when primary damage is created in displacements. Indeed more than 99% of the point defects are created in an isolated way. The production rate can be calculated with a good accuracy [13].

2.2.2. Recombination rate of point defects

This is given by

$$R_{iv} = 4\pi r_{iv}(D_i + D_v), \tag{6}$$

where $D_\theta = D_{\theta 0}\exp(-E^{m}_{\theta}/kT)$ is the diffusion coefficient of the point defect of type $\theta = i, v$ with $D_{\theta 0}$ the frequency factor, E^{m}_{θ} the migration energy and r_{iv} the recombination radius that we will take equal to $2.5a$ where a is the lattice parameter.

2.2.3. Rate coefficient for dislocations

The more sophisticated models consider explicitly the drift interaction between the point defect and the dislocation but are difficult to include simply in a rate equation model. This interaction is frequently included by assigning a capture radius which depends on the nature of the point defect. We have per unit length of dislocation

$$K^{d}_{\theta}C_{1\theta} = \rho Z^{d}_{\theta}D_\theta C_\theta, \tag{7}$$

where ρ is the dislocation density and Z_θ^{d} the capture efficiency which in theory depends on the rate of capture of the point defect by all the sinks either of same type or not present in the medium (multiple sinks effect). If we ignore the multiple-sink correction due to other sinks except dislocation, a multiple-sink term remains in the zero order expression [10]

$$Z_\theta^{\mathrm{d}} = \frac{2\pi}{\ln(1/r_\theta^{\mathrm{d}}\sqrt{\pi\rho})}. \tag{8}$$

As ρ is in the argument of the logarithm, we will consider in practice that Z_θ^{d} is a constant independent of ρ but not of the trapping radius of the dislocation r_θ^{d}. Usually $Z_{\mathrm{v}}^{\mathrm{d}}$ is taken equal to one and $Z_{\mathrm{i}}^{\mathrm{d}} = (1+\varepsilon)Z_{\mathrm{v}}^{\mathrm{d}}$ with ε around 0.2.

2.2.4. Rate coefficients for clustering

These rate coefficients for clustering of dislocation loops have been the topic of a great number of studies which are often not in good or even in fair agreement with each other. The simplest models do not consider explicitly the drift interaction. The more sophisticated ones take it into account [14,15]. In some cases, special effects such as the polarizabilities of the point defects [16], non-linear elasticity [17], or the saddle-point shape anisotropy of point defects [18] are considered.

We will discuss them briefly in order to justify our choice. To be easily included in the model, the rate coefficient must be given by an analytical expression. This eliminates most of the approaches that take explicitly into account the drift term. Furthermore, the expression must be valid over the whole range of n. This implies, as pointed out by Stoller [19], that the expression for $\beta_{n\theta}^{\theta'}$ is subject to two important constraints. The first is that for large values of loop radius it must be in agreement with the one for dislocations and the second is that for $n = 1$ it must be in agreement with the one given by the atomistic, combinatorial method.

The simplest approach considers that the rate of point defects capture of a dislocation loop of radius r_n is equal to the rate of point defects capture of a straight dislocation whose length is the same as the perimeter of the dislocation loops [20]:

$$\beta_{n\theta}^{\theta'} C_{\theta'} = 2\pi r_n Z_{n\theta}^{\theta'} D_{\theta'} C_{\theta'}, \tag{9}$$

where

$$r_n = \left(\frac{nV_{\mathrm{at}}}{\pi b}\right)^{1/2} \tag{10}$$

with $Z_{n\theta}^{\theta'} = Z_{\theta'}^{\mathrm{d}}$ hence independent of r_n and θ, V_{at} the atomic volume and b the Burgers vector of the loop assumed to be prismatic.

To compare easily the various expressions of the rate coefficient for clusters, it is also interesting to introduce the equivalent spherical capture radius of a loop $r_{n\theta}^{\theta'}$ defined by

$$\beta_{n\theta}^{\theta'} C_{\theta'} = 4\pi r_{n\theta}^{\theta'} D_{\theta'} C_{\theta'}. \tag{11}$$

(9) and (11) fulfil the first constraint but not the second. Indeed, with the iron lattice parameter and $Z_\theta^{\mathrm{d}} = 1$ ($\theta = \mathrm{v}$), (9) and (11) give $Z_{1\theta}^{\mathrm{v}} = 1$ ($r_{1\theta}^{\mathrm{v}} = 0.12$ nm) when the combinatorial method gives $Z_{1\theta}^{\mathrm{v}} = 6.7$ ($r_{1\theta}^{\mathrm{v}} = 0.45$ nm).

A better approach is to take into account the toroïdal shape of a circular dislocation loop [21]. We have again

$$\beta_{n\theta}^{\theta'} C_{\theta'} = 2\pi r_n Z_{n\theta}^{\theta'} D_{\theta'} C_{\theta'} \tag{12}$$

but now $Z_{n\theta}^{\theta'}$ is not a constant anymore but depends on the radius of the loop (geometrical effect)

$$Z_{n\theta}^{\theta'} = \frac{2\pi}{\ln(8r_n/r_{\mathrm{p}})}, \tag{13}$$

where r_{p} is the pipe radius.

Assuming $r_{\mathrm{p}} = 2b$ and $b = 0.2$ nm, we have now $Z_{1\theta}^{\mathrm{v}} = 6.3$ ($r_{1\theta}^{\mathrm{v}} = 0.43$ nm) in fair agreement with the combinatorial method (for vacancies since drift interaction is neglected). However the first constraint is not fulfilled since $Z_{n\theta}^{\theta'}$ tends towards zero when $r_n \to \infty$.

In order to satisfy both constraints we finally propose the following expression:

$$Z_{n\theta}^{\theta'} = Z_{\theta'}^{\mathrm{d}} + \left[\left(\frac{b}{8\pi a}\right)^{1/2} z_{\theta'} - Z_{\theta'}^{\mathrm{d}}\right] \Big/ n^{\gamma_{\theta'}/2}, \tag{14}$$

where a is the lattice parameter.

By adjusting properly $z_{\theta'}$ and $\gamma_{\theta'}$, (14) fits well the curve for vacancy capture given by (13) for not too large n values ($z_{\mathrm{v}} = 35$, $\gamma_\theta^{\mathrm{v}} = 0.7$). Fig. 1(a) shows how these curves fit. In the case of interstitials, we will assume that $Z_{n\theta}^{\mathrm{i}}/Z_{n\theta}^{\mathrm{v}}$ is a constant equal to $Z_{\mathrm{i}}^{\mathrm{d}}/Z_{\mathrm{v}}^{\mathrm{d}}$ which gives $z_{\mathrm{i}} = 42$, $\gamma_{\mathrm{i}} = 0.7$. It is worth noting that (14) gives $Z_{n\mathrm{i}}^{\theta'} = Z_{n\mathrm{v}}^{\theta'}$. Fig. 1(a) and (b) shows $Z_{n\theta}^{\theta'}$ versus r_n for vacancies and interstitials given by (9), (13) and (14) with $Z_{\mathrm{v}}^{\mathrm{d}} = 1$, $Z_{\mathrm{i}}^{\mathrm{d}} = 1.2$. These figures also show the curves given by Coghlan and Yoo [14] with the corresponding fit given by (14) ($z_{\mathrm{v}} = 42$, $\gamma_{\mathrm{v}} = 0.8$, $z_{\mathrm{i}} = 56$, $\gamma_{\mathrm{i}} = 0.65$) in the range of validity of the Coghlan theory (approximately 2 nm $< r_n <$ 100 nm) and the curve given by [16]. Except for the curve given by (9), it is clear that all the curves but the ones given by the Wolfer model [16] are similar. In the latter case, Z decreases considerably more rapidly with r, than in the other cases. We finally used (14) in our work $z_{\mathrm{v}} = 35$, $\gamma_{\mathrm{v}} = 0.7$ for vacancies and $z_{\mathrm{i}} = 42$, $\gamma_{\mathrm{i}} = 0.7$ for interstitials.

It is worth noticing that an equation similar to (14) was already used in a rate equation modelling [19] but with $\gamma_{\mathrm{i}} = \gamma_{\mathrm{v}} = 2$ as in [16].

In good agreement with what is often admitted, (14) gives $\beta_{n\theta}^{\theta'}\Big|_{\theta\neq\theta'} = \beta_{n\theta}^{\theta'}\Big|_{\theta=\theta'}$. This leads to an inconstancy for

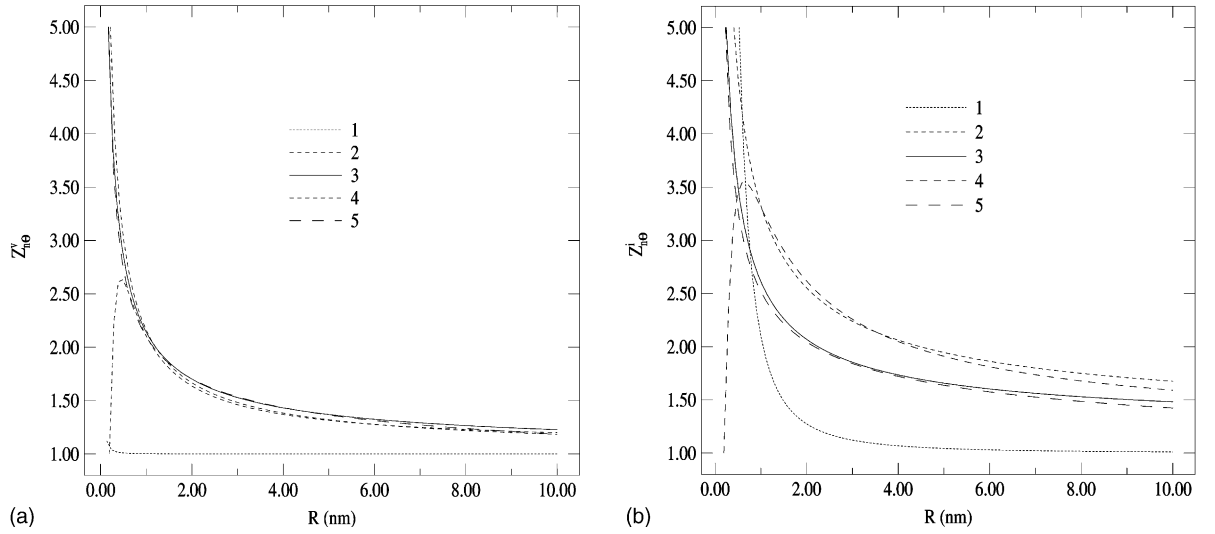

Fig. 1. Capture efficiency of dislocation loops versus their radius (a) for vacancies and (b) for interstitials. Curve 1, given by Wolfer and Ashkin [16]; curve 2 given by (14) with $Z_{\mathrm{v}}^{\mathrm{d}} = 1$, $z_{\mathrm{v}} = 42$, $\gamma_{\mathrm{v}} = 0.8$, for vacancies and $Z_{\mathrm{i}}^{\mathrm{d}} = 1.2$, $z_{\mathrm{i}} = 56$, $\gamma_{\mathrm{i}} = 0.65$ for interstitials; curve 3 given by (14) with $z_{\mathrm{v}} = 35$, $\gamma_{\mathrm{v}} = 0.7$ for vacancies and $z_{\mathrm{i}} = 42$, $\gamma_{\mathrm{i}} = 0.7$ for interstitials; curve 4 given by Coghlan and Yoo [14] and curve 5 given by Seeger and Gösele [20].

low n if $r_{n\theta}^{\theta'} < r_{\mathrm{iv}}$ since the capture radius of an interstitial by a vacancy cluster (respectively the capture radius of a vacancy by an interstitial cluster) cannot be smaller than r_{iv}. Fig. 2 shows that this problem actually appears for a reasonable value of $r_{\mathrm{iv}} = 0.65$ nm, especially if we consider the case where $Z_{n\theta}^{\theta'} = Z_{\theta'}^{\mathrm{d}}$. So we will take $r_{n\theta}^{\theta'} = r_{\mathrm{iv}}$ if $r_{n\theta}^{\theta'} < r_{\mathrm{iv}}$.

The rate of emission of a point defect by a cluster $\alpha_{n\theta}^{\theta}$ is obtained by considering that the detail balance applies separately for vacancy and for interstitial. Then

$$\alpha_{n\theta}^{\theta} = 2\pi r_{n-1} Z_{(n-1)\theta}^{\theta} D_{\theta} \exp(-E_{n\theta}^{\mathrm{B}}/kT) \tag{15}$$

with $E_{n\theta}^{\mathrm{B}} = E_{\theta}^{\mathrm{f}} - (E_{n\theta}^{\mathrm{f}} - E_{(n-1)\theta}^{\mathrm{f}})$ the binding energy of the point defect θ with the cluster $n\theta$ where E_{θ}^{f} and $E_{n\theta}^{\mathrm{f}}$ are

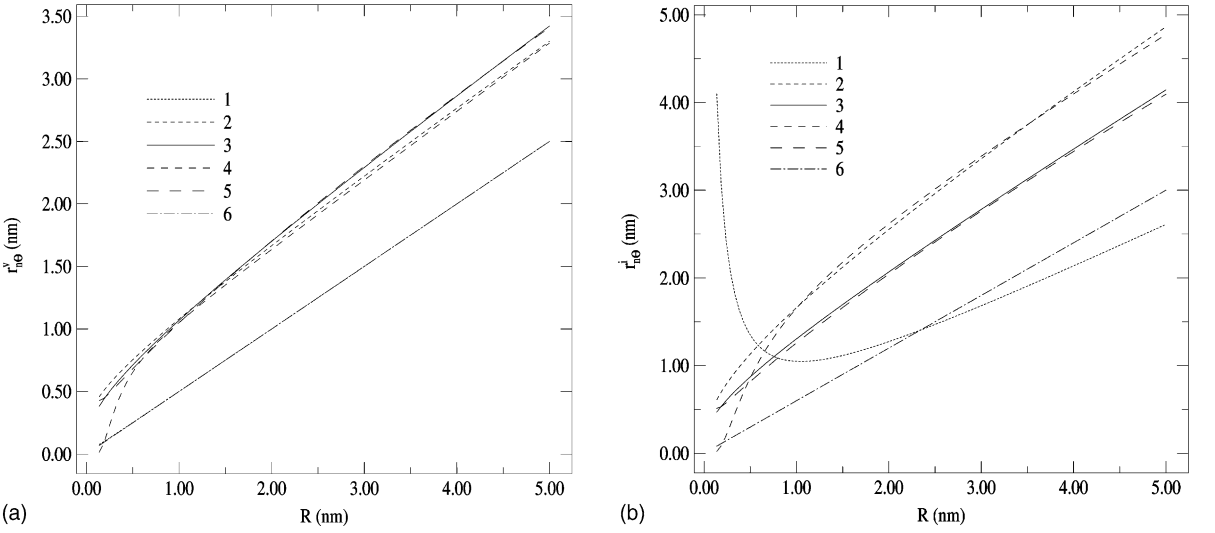

Fig. 2. Capture radius of dislocation loops versus their radius (a) for vacancies and (b) for interstitials. The definitions of the curve are the same as in Fig. 1. Curve 6 corresponds to the very simple case where $Z_{n\theta}^{\theta'} = Z_{\theta'}^{\mathrm{d}}$. In (a), there is almost no difference between curve 1 and 6.

the formation energies of the point defect θ and of the cluster $n\theta$ respectively.

It has been shown by molecular dynamic simulation that in iron [22]

$$E^{B}_{n\theta} = E^{f}_{\theta} + \frac{E^{B}_{2\theta} - E^{f}_{\theta}}{2^{\sigma} - 1}\left[n^{\sigma} - (n-1)^{\sigma}\right] \tag{16}$$

with $\sigma = 2/3$.

The number of parameters needed to describe $E^{B}_{n\theta}$ is then reduced to two for each type of point-defect cluster.

Fig. 3 shows that, for large n, (16) is in reasonably good agreement with the expression given by the elastic theory of dislocations neglecting an eventual contribution of a staking fault [23]

$$E^{B}_{elas} = E^{f} - \frac{\mu b^4}{4\pi(1-\nu)r}\ln\left(\frac{32r}{b}\right). \tag{17}$$

Concerning α^{v}_{xi} we will take

$$\alpha^{v}_{xi} = 2\pi r_{x-1} Z^{v}_{(n-1)v} D_v \exp(-E^{B}_{xv\_i}/kT)$$

with $E^{B}_{xv\_i} = E^{f}_{v} + \frac{E^{f}_{i} - E^{B}_{2i}}{2^{2/3}-1}\left[x^{2/3} - (x-1)^{2/3}\right]$.

2.2.5. Rate coefficients for surfaces and grains boundaries

The multiple sink effect is no more a simple correction and cannot be ignored. We used the expressions given by Bullough et al. [24].

In fact the microstructure is very often such that a simplest expression can be used. Let us define the sink strength S^{sk}_{θ} of a sink sk for the point defect of type $\theta = i, v$ as usually by

$$K^{sk}_{\theta} C_{\theta} = S^{sk}_{\theta} D_{\theta} C_{\theta}. \tag{18}$$

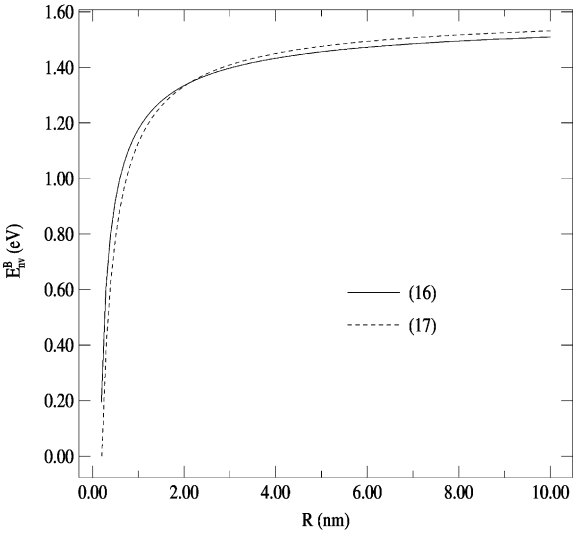

Fig. 3. Binding energy of a vacancy with a vacancy loop versus the size of the loop calculated by using (16) and (17).

If S^{sc}_{θ} is the sum of the sink strengths of all the sinks but the grain boundary (or the surface) and λ the size of the grain d (or L the thickness of the thin foil), the microstructure quickly become such that $(S^{sc}_{\theta})^{1/2}\lambda$ is very large. Then S^{sk}_{θ} is given by

$$S^{sk}_{\theta} = (S^{sc}_{\theta})^{1/2} H \tag{19}$$

with $H = 6/d$ for a grain boundary and $H = 1/L$ for a thin foil.

3. HVEM irradiation experiments [25]

They were carried out in two low copper content alloys, FeCu (0.13 wt%) and FeMn(1.5 wt%)Ni(0.8 wt%)Cu(0.13 wt%)P(0.01 wt%) hereafter called the complex alloy and non-alloyed Fe for comparison. The main impurities are 0.2 at.%Al, 0.04 at.%Si, 0.012 at.%S and 0.02 at.%P. Furthermore, all these alloys contain 20 wppm carbon to take into account the important effect of carbon in ferritic steels on the mobility of vacancies [26]. The ingots were cold-rolled up to 0.2 mm. The sheets were then annealed in vacuum for 24 h at 820 °C.

Irradiations were performed in the 1 MeV Transmission Electron Microscope of CEA-Saclay. Discs of 3 mm were punched out of the foils and electrolitically jet-polished in a 5% $HClO_3$ and 95% C_2H_5OH solution at 30 V and −70 °C. The irradiations were carried out using a double-tilt heating specimen holder. In order to prevent any oxidation, the vacuum in the vicinity of the specimen is kept below 5×10^{-8} Torr. The purpose of these experiments was to measure the evolution with temperature of the saturation density of dislocation loops and if possible, the growth rate of the dislocation loops. The nature of the loops was not analysed but within the experimental conditions they are known to be of interstitial type.

3.1. The number density

The saturation number density of interstitial dislocation loops D_{sat} is the principal quantity considered in the modelling. The measurements of D_{sat} were carried out in the following way: after inserting the sample holder in the microscope a suitable grain is quickly selected using a very low electron current density so that no loops nucleate. The sample is then shifted so that the electron beam passes entirely through the hole in the sample, the specimen cradle heated to the lowest temperature and the electron current density adjusted to 4×10^{18} e cm^{-2} s^{-1} which corresponds to a displacement rate of 1.5×10^{-4} dpa/s. The selected zone is shifted back again under the beam to start the irradiation. The irradiation is performed until we judge that the density of loops has become constant. In practice, the irradiation time was around 15–20 min. The sample is then

shifted towards a virgin area and heated again to reach the next temperature. The procedure is repeated up to the highest temperature. The irradiation is performed preferably in the same grain if it is large enough. By the end of the experiment carried out at the highest temperature a micrograph of the lowest temperature area is taken to check that its microstructure has not changed during the irradiation of the other areas at highest temperature.

After irradiation, classical TEM observations were carried out to determine the number density of dislocation loops. The images were taken under two-beam-kinematical-bright-field conditions with a diffraction vector of type $g = \{1\,1\,0\}$. Images obtained after irradiation at low and high temperatures for the three materials are given in Fig. 4. By using the thickness fringes, a map of the thickness of irradiated areas is obtained. For this purpose a two-beam-bright-field image under dynamical condition was also taken. The number density of loops per surface unit in each region of equal thickness corresponding to the fringes was measured. The loop density $N_{\mathrm{li}}^{\mathrm{st}}$ is given by the relation

$$N_{\mathrm{li}}^{\mathrm{st}} = N_{\mathrm{surf}}/(e - 2\zeta_{\mathrm{d}}), \tag{20}$$

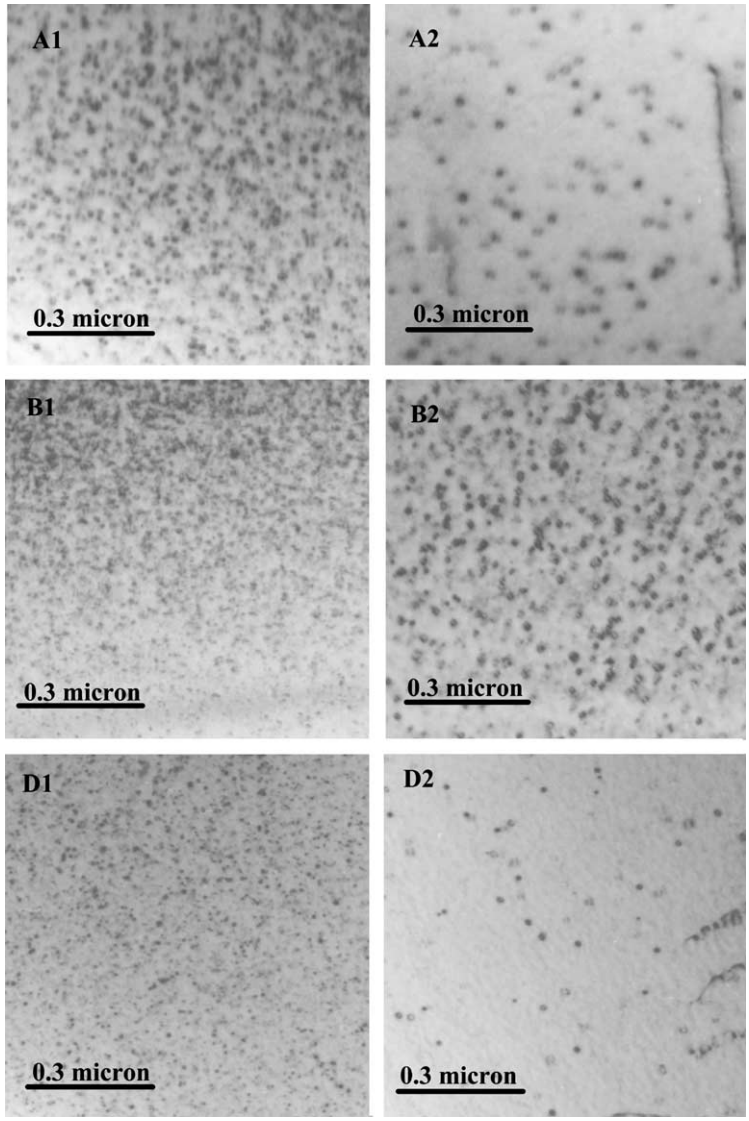

Fig. 4. Images of interstitial dislocation loops taken under two beams kinematical bright field conditions with a diffraction vector of the type $g = \{1\,1\,0\}$. A1: Iron, 217 °C, 12 mn. A2: Iron, 364 °C, 27 mn. B1: FeCu, 170 °C, 15 mn. B2: FeCu, 351 °C, 45 mn. D1: Complex alloy, 306 °C, 14 mn. D2: Complex alloy, 392 °C, 14 mn.

where N_{surf} is number of loops per surface unit, ζ_d is thickness of the depleted zone and e is local thickness of the thin foil. By plotting N_{surf} as a function of e, we obtain the value of N_{li}^{st} and ζ_d for the temperature at which the irradiations were performed.

Fig. 5 shows a plot of $\ln N_{li}^{st}$ versus $1/T$ where T is the irradiation temperature, for the three materials. The plotted points are related to two grains in two different samples for the complex FeMnNiCuP alloy, to one grain in the FeCu alloy and to three grains in two different samples for Fe.

The FeCu alloy shows an Arrhenian behaviour over the whole range of temperature.

Non-alloyed Fe gives a small slope at low temperature and a large slope at the highest temperature. Several extra experiments, not plotted in this graph, were carried out on thickest thin foils to check if the slop transitions near 300 °C is not simply a thickness effect. The answer is no since in every case the same behaviour is observed.

Concerning the complex alloy, if we omit the highest temperature point, N_{li}^{st} follows an Arrhenius law with an energy as high as 6 eV.

It is worth noting that because of the small size of the loops, the N_{li}^{st} values obtained at the lowest temperature for Fe and FeCu are lowerbounds.

Simple models are often used to derive the interstitial mobility from the change of N_{li}^{st} with T [27–29]. They are based on drastic approximations: the di-interstitial is the loop nucleus, vacancies are motionless... With our notations N_{li}^{st} is then given by

$$N_{li}^{st} = \left(\frac{G}{(12\pi r_{iv} + 4\pi r_1 Z_{2i}^{i}) D_{i0}}\right)^{1/2} \exp\left(-\frac{E_i^m}{2kT}\right). \quad (21)$$

Eq. (21) applied to our experimental results gives $E_i^m = 0.3$ eV for FeCu and 3 eV for the complex alloy. If the former value is in good agreement with the experimental results for Fe given in the literature by using various methods [30], the latter is too high to have any physical meaning. It must be concluded that (21) can not be applied to the complex alloy. Concerning Fe, it is difficult to use (21). However if we remember that N_{li}^{st} for the point at the lowest temperature is lowerbound and that experimental errors are larger than for highest temperatures we can write $0.1 < E_i^m < 0.3$ eV.

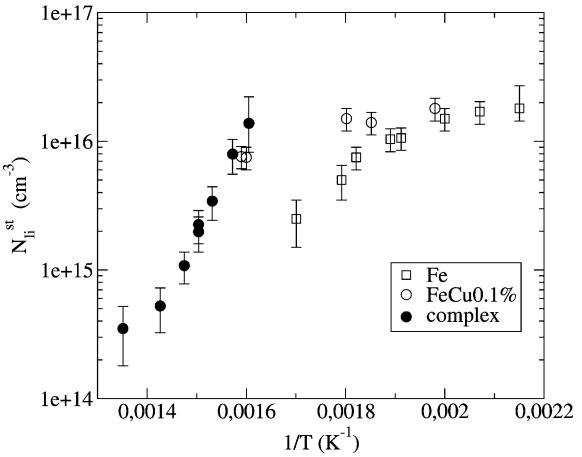

Fig. 5. Logarithm of D_{sat}, the saturation number density of interstitial dislocation loops, versus $1/T$, for the three materials.

If (29) is applied to FeCu with Z_{2i}^{i} given by (13), a rough estimation of the frequency factor of the diffusion coefficient of interstitials is $D_{i0} = 5 \times 10^{-5}$ cm^2/s. The size distribution is also interesting to consider as a validation of the modelling even if the determination is not precise because of the small size of the loops. Indeed, to obtain a large range of N_{li}^{st}, the size must be necessary small if we want to avoid any interaction between dislocation loops. Some size distributions of interstitial loops are given on Fig. 6. It is worth noting that it was not possible to obtain such a histogram for all the experiments especially in the case when the loops are to small. Then, only estimations of the mean size were carried out. These values are certainly lowerbounds if we consider the faint contrast given by electron microscopy for very small loops.

3.2. Growth rate

The experimental procedure is almost the same but the electron flux is six times larger and the temperature range higher (from 300 to 600 °C). At the highest temperatures, when the nucleation rate is to small to observe any loops in the irradiated area, the loops are nucleated at lower temperature. To minimise the effect of the surfaces, the experiments are carried out in zones as thick as possible regarding the quality of the image which are recorded on tapes using a video device. The diameters or the largest dimension of the loops when they are not circular is subsequently measured as a function of time. A linear behaviour is always observed. So, a growth rate can easily be obtained. Fig. 7 shows an Arrhenius plot of the growth rate of loops in iron obtained on a single thin foil. The solid line corresponds to points (black squares) obtained by increasing the temperature on a fresh sample from room temperature up to 600 °C and the dash line to points (empty circles) obtained by decreasing the temperature on the same sample. Subsequent increase or decrease carried out on the same sample gave points that remain on dash line. If the point-defect concentration is controlled by recombination and the sink strength of surfaces significantly higher than the sink strength of the loops (low number density of loops), the stationary growth velocity is given by

$$\frac{dR_l}{dt} = \frac{2}{b}\left(Z_i^l - Z_v^l\right)\left(\frac{GV_{at}D_{v0}}{4\pi r_{iv}}\right)^{1/2} \exp\left(-\frac{E_v^m}{2kT}\right), \quad (22)$$

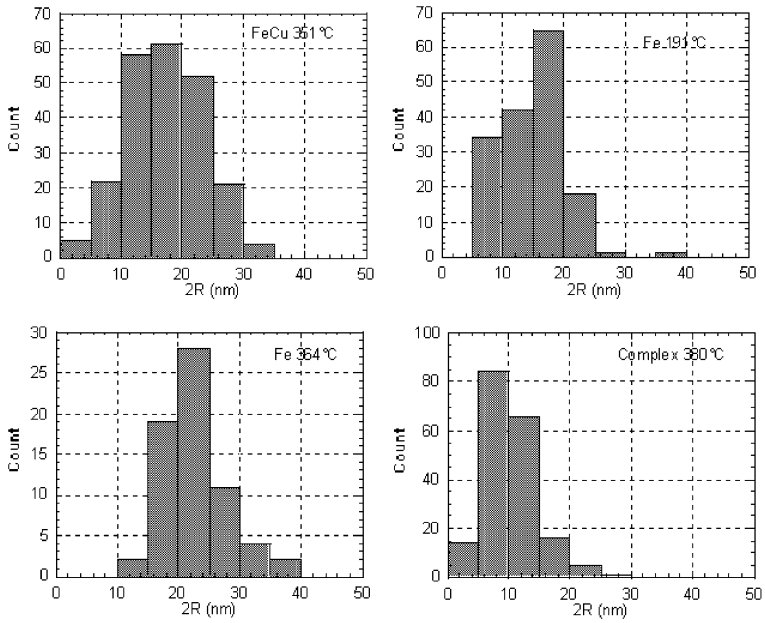

Fig. 6. Size distributions of interstitial loops obtained by the end of experiments carried out at 1.5×10^{-4} dpa/s. After 17 mn at 191 °C and 25 mn at 364 °C in iron, 18 mn at 351 °C in FeCu and 15 mn at 380 °C in the complex alloy.

where Z_θ^{l} is the capture efficiency of loops. As the size of the loops experimentally measured is larger than 10 nm it is reasonable to assume in (22) that $Z_\theta^{\mathrm{l}} \approx Z_\theta^{\mathrm{d}}$.

The $E_{\mathrm{v}}^{\mathrm{m}}$ and a rough estimation of $D_{\mathrm{v}0}$ effective values can be derived from (22). We have $E_{\mathrm{v}}^{\mathrm{m}} = 1.36$ eV, $D_{\mathrm{v}0} = 5$ cm^2/s by the first rise of the temperature and then $E_{\mathrm{v}}^{\mathrm{m}} = 0.73$ eV, $D_{\mathrm{v}0} = 5$ cm^2/s. These $E_{\mathrm{v}}^{\mathrm{m}}$ values are very close to those given by others [26] for respectively standard and ultra-pure iron. It is often assumed that the high value comes from the deep trapping of vacancies by interstitial carbon resulting in the formation of immobile complexes. Actually the best interpretation of our results is to assume that carbon or some other impurity trapping the vacancies had left the thin foil during the first heating at 600 °C.

The same behaviour is observed in FeCu.

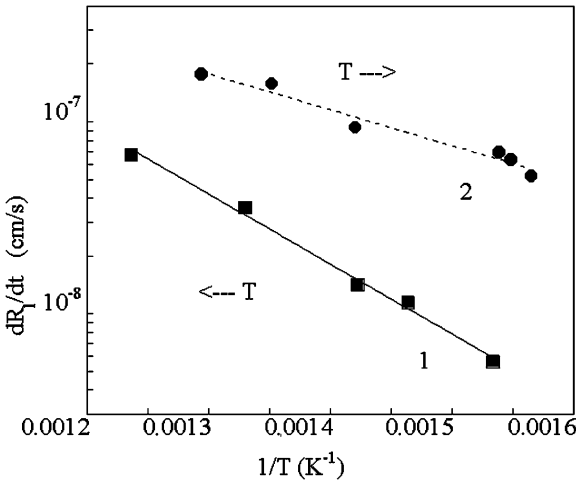

Fig. 7. Arrhenius plot of the growth rate of interstitial dislocation loops in iron obtained on a single thin foil. The dash line corresponds to points (black squares) obtained by increasing the temperature up to 600 °C and the solid line to points (empty circle) obtained by decreasing the temperature on the same sample.

4. Research of a good set of parameters and discussion

Our purpose is to find the best set of parameters able to reproduce the stationary number density of interstitial loops $N_{\mathrm{li}}^{\mathrm{st}}$. We will also consider the size of these loops measured or estimated by the end of the experiments carried out to measure $N_{\mathrm{li}}^{\mathrm{st}}$.

Many parameters concerning pure iron have been studied experimentally or by atomic simulation. So the range within which they can vary is limited.

We will first discuss the parameters for pure iron; present the results given by the model with a reference set of parameters and show how they must be changed to improve the fit. We will then consider FeCu and complex alloys.

4.1. Pure α iron

Due to the phase transition and the magnetism, reliable experimental values for vacancy formation and

migration are difficult to obtain. That is why a controversy still remains about E_v^m (a group of values is around 1.3 eV and an other around 0.6 eV [26,30]). The vacancy formation energy E_v^f is given between 1.6 and 2.0 eV [30]. Atomistic simulations on the other hand give a large range of values for E_v^m from 0.11 to 1.45 eV depending on the inter-atomic potential and $1.4 < E_v^f < 2.1$ eV. Concerning interstitials, experimental measurements give $0.25 < E_i^m < 0.3$ eV [30] and atomistic calculations lower values between 0.15 and 0.30 eV [22,31,32]. No experimental E_i^f values exist while simulations give $3 < E_i^f < 7$ eV [22,30–34].

The parameters E_{2v}^B and E_{2i}^B entering in (16) are given only by atomistic simulations. Fits of molecular dynamic simulation carried out by Soneda and Diaz de la Rubia [22] give $E_{2v}^B = 0.23$ eV and $E_{2i}^B = 0.71$ eV.

Considering the values given by the literature and our experimental data, a reference set of parameters was finally chosen. It is given in Table 1. The migration energies of point defects are those given by the simplified models applied to our HVEM experiments on fresh thin iron foils. The frequency factors have been changed for reasons that will be given below. The dose rate, the temperature range and the foil thickness are those used in our experiments carried out to measure the number density of loops.

Fig. 8 gives a typical evolution of the distribution of interstitial loops at low temperature (181 °C) with the reference set of parameters. As expected, a well-defined peak appears quickly for small values of t. It then shifts towards the larger loop sizes while spreading out. At the left side of the peak a stationary distribution appears which decreases rapidly from $n = 1$ and does not change any more when the peak shifts towards large r values. From the calculated loops distribution a number density of loops N_{li} is obtained. To compare with experiments, only loops above a radius of 0.65 nm ($n = 20$) corresponding approximately to the experimental limit of observation are considered. The evolution of N_{li} at 181 °C is given on Fig. 9. After 1 s, N_{li} reaches a plateau N_{li}^{st}. Fig. 9 also shows that D_{0i} (4×10^{-3} and 5×10^{-5} cm^2 s^{-1}) has an important effect on N_{li}^{st}. In fact it is, at low temperature, the most sensitive parameter.

Table 1

Symbol	Value
G	1.5×10^{-4} dpa/s
T	$175 < T < 400$ °C
L	0.3 μm
E_v^m	1.3 eV
E_v^f	1.6 eV
D_{v0}	1 cm^2/s
E_i^m	0.3 eV
E_i^f	4.3 eV
D_{i0}	4×10^{-4} cm^2/s
r_{iv}	0.65 nm
ρ	1×10^8 cm/cm^3
Z_v^d	1.0
Z_i^d	1.2
$z_{1\theta}^v$	35
$z_{1\theta}^i$	42
γ_θ^v	0.7
γ_θ^i	0.7
E_{2v}^B	0.2 eV
E_{2i}^B	0.8 eV
N_i	20
N_{iC}	180
N_v	300
N_{vC}	0
C_{xi}	1.05

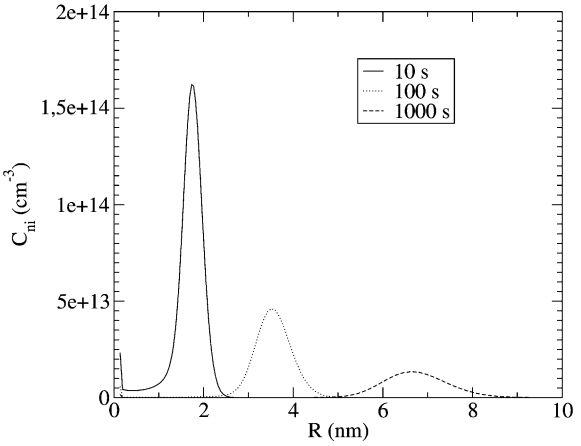

Fig. 8. Typical evolution of the distribution of interstitial loops at low temperature (181 °C) with the reference set of parameters.

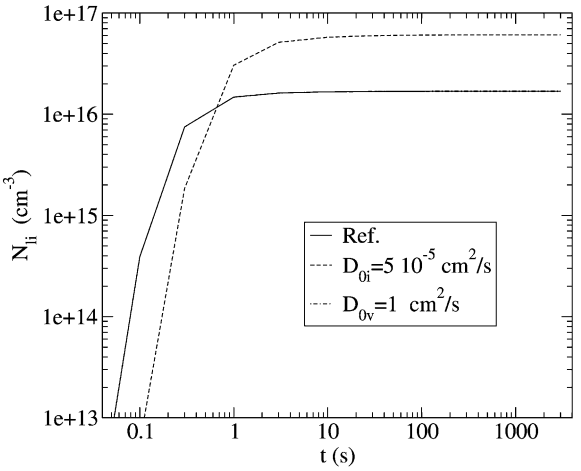

Fig. 9. Evolution of the number density of interstitial loops N_{li} at 181 °C. The curves which correspond to $D_{0v} = 1$ and 5 cm^2/s are superimposed.

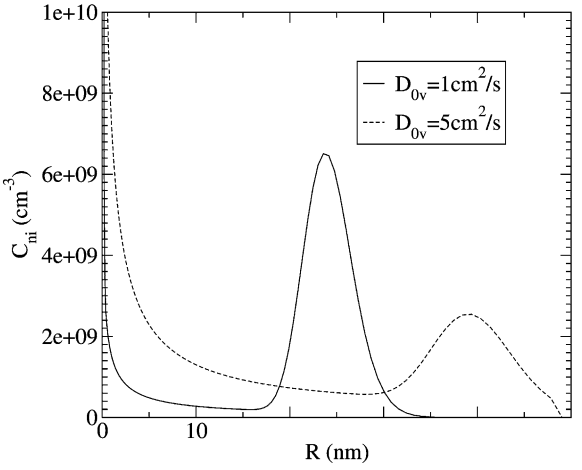

Fig. 10. Distribution of interstitial loops at high temperature (352 °C), after 1000 s, calculated by using the reference set of parameters and effect of D_{0v}.

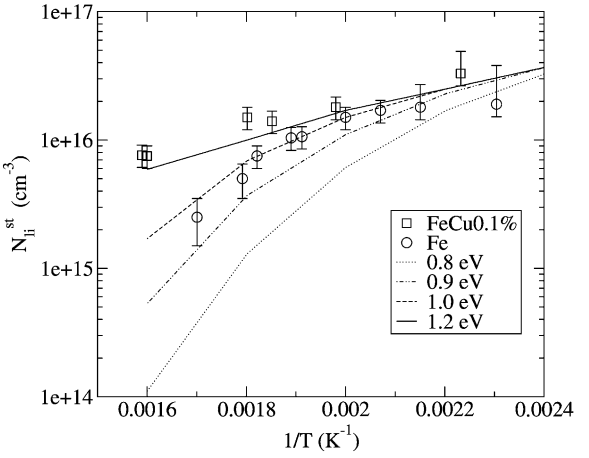

Fig. 11. Comparison of $\ln N_{\mathrm{li}}^{\mathrm{st}}$ calculated with the reference set of parameters and various values of $E_{2\mathrm{i}}^{\mathrm{B}}$ versus $1/T$ with the experimental results obtained in Fe and FeCu.

Fig. 10 gives the distribution of interstitial loops at high temperature (352 °C), after 1000 s, calculated by using the reference set of parameters. On the same figure is also given the distribution with the same set of parameters except $D_{0\mathrm{v}}$ which is five times greater (the rough value extracts from our experiments by using value given by (21)). With the latter value, the shift toward the right of the peak is, as expected greater and the size of the loops too large. The reason of this behaviour is simply that when the stationary state for point defect is reached, the growth rate of the loops increases with D_{v}, as shown by (21). Secondly, the peak does not emerge totally any more from the stationary distribution in disagreement with what is observed experimentally.

The comparison of $\ln N_{\mathrm{li}}^{\mathrm{st}}$ (calculated with the reference set of parameters) versus $1/T$ with the experimental value shows qualitatively a good behaviour (Fig. 11) but the rapid decrease at high temperature is slightly too important. Calculations with various value of $E_{2\mathrm{i}}^{\mathrm{B}}$ show clearly that the high slope is due to the ability of clusters to emit interstitials. This fact was already pointed out by Bourret [28]. If we remember that the point at the lowest temperature are lowerbounds with a large experimental error, we can consider that the experimental $N_{\mathrm{li}}^{\mathrm{st}}$ curve is correctly fitted with $E_{2\mathrm{i}}^{\mathrm{B}} = 0.9$ eV.

4.2. FeCu alloy

We will consider that the basic Eqs. (2) and (3) remain valid for the alloy which are now considered as effective media or as 'grey metals'. The parameters describing the mobility of point defects and the stability of clusters must now be considered as effective parameters. This can be justified for the point-defect mobility if the temperature is not too low because in this case the local equilibrium is satisfied (for example between free point defects, free solute atoms and solute-defect pairs in the case of a dilute alloy). This is nothing but the basic assumption of mater transport theory in solids [35]. Considering the formation energy of clusters, it is simply an assumption. We will consider that the relation (16) still remains valid. The only effect of the solutes is then to modify the value of $E_{2\theta}^{\mathrm{B}}$ and possibly the one of E_{θ}^{f}. Obviously, a possible effect of segregation of solute atoms on the point-defect clusters is not explicitly considered.

The experimental values of $N_{\mathrm{li}}^{\mathrm{st}}$ can be fitted with the same parameters as for the non-alloyed Fe except the $E_{2\mathrm{i}}^{\mathrm{B}}$ value, which must satisfy $E_{2\mathrm{i}}^{\mathrm{B}} \geqslant 1.2$ eV (Fig. 11). The presence of copper atoms stabilised the small interstitial clusters. Indeed the $N_{\mathrm{li}}^{\mathrm{st}}$ values are slightly too small. They could be easily pushed up by very slightly decreasing $D_{\mathrm{i}0}$.

4.3. The complex alloy

By considering Fig. 5, it is clear that the set of parameters for this alloy, the composition of which is close to those of the ferrite of actual steels, is very different from the set used to fit $N_{\mathrm{li}}^{\mathrm{st}}$ for Fe and the FeCu binary alloy. To find a good set, we have considered that the high slope observed experimentally has the same origin as the high temperature slope observed for iron but with parameters such as the $N_{\mathrm{li}}^{\mathrm{st}}$ values at low temperature, where the slope is small, are too high to be measured experimentally. Then, compared to the set of parameters for Fe, $E_{2\mathrm{i}}^{\mathrm{B}}$ must then be smaller to get a rapid decrease of the curve at high temperature and D_{i} must be significantly smaller too to obtain very high $N_{\mathrm{li}}^{\mathrm{st}}$ values at low temperature. Fig. 12 shows that experimental points

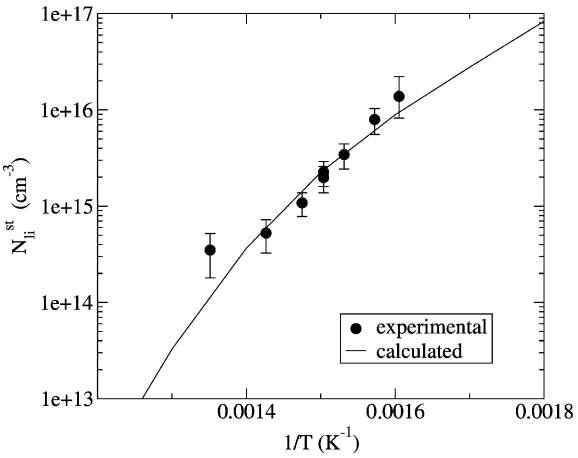

Fig. 12. Comparison of the calculated values of $\ln N_{\mathrm{li}}^{\mathrm{st}}$ versus $1/T$ with the experimental results obtained in the complex alloy.

can be fitted with $E_{\mathrm{i}}^{\mathrm{m}} = 1.0$ eV, $D_{0\mathrm{i}} = 4 \times 10^{-3}$, $D_{0\mathrm{v}} = 10^{-2}$ and $E_{2\mathrm{i}}^{\mathrm{B}} = 0.2$ eV, the other parameters being those used for Fe.

It is worth noting that a simple model [28] considers the possibility of dissociation of di-interstitials and predicts an activation energy at high temperature equal to $(5E_{\mathrm{i}}^{\mathrm{m}} + 4E_{2\mathrm{i}}^{\mathrm{B}})/6$ which gives 0.8 eV in total disagreement with what we obtained. The reason is probably that the model used here considers not only the dissociation of di-interstitials but also the one of larger clusters. The mobility of vacancies could also play a role.

5. Conclusion

In this article we have reported the first step of a project devoted to the modelling of the component of hardening of pressure vessels due to point-defect cluster. For this purpose a rate equation model has been developed and applied to a simple binary alloy FeCu (0.13 wt%), a complex alloy FeMn(1.5 wt%)Ni(0.8 wt%) Cu(0.13 wt%)P(0.01 wt%) the composition of which is close to the one of the matrix of pressure vessel steels and non-alloyed Fe for comparison. The calibration of the model was obtained by carrying out 1 MeV electron irradiations in these materials and by using the results of experiments and atomic simulations reported in the literature. The main results are:

(i) the presence of copper in iron do not affect the mobility of interstitial but stabilises the interstitial clusters since the binding energy of di-interstitials must be increased from 0.9 eV for iron to a value equal or larger than 1.2 eV.
(ii) the parameters relative to the interstitials in the complex alloy are totally different from these for iron: the apparent migration energy is now around 1 eV and the binding energy of di-interstitials as low as 0.2 eV. This important result shows that parameters obtained by numerical simulation on pure iron or even on low copper binary alloys can not be used directly for modelling the hardening of actual pressure vessel steels except if it is proofed that under neutron irradiation free interstitials do not play any role.
(iii) the parameters relative to the vacancy are not significantly affected by the alloying elements.

Acknowledgements

The authors deeply grateful Dr P. Dubuisson for their kind help in the use of the high voltage electron microscope.

References

[1] G.R. Odette, G.E. Lucas, in: L.E. Steele (Ed.), ASTM STP 909, American Society of Testing and Materials, Philadelphia, PA, 1986, p. 206.
[2] P. Auger, P. Pareige, M. Akamatsu, J.C. Van Duysen, J. Nucl. Mater. 211 (1994) 194.
[3] A. Hempel, M. Hasegata, G. Brauer, F. Plazaola, M. Saneyasu, Z. Tang, 9th Conf. On Environmental Degradation of Materials in Nuclear Power Systems – Water Reactors, 1999.
[4] A. Barbu, M.H. Mathon, F. Maury, J.F. Belliard, B. Beuneu, C.H. de Novion, J. Nucl. Mater. 257 (1998) 206.
[5] M. Akamatsu, J.C. Van Duysen, P. Pareige, P. Auger, J. Nucl. Mater. 225 (1995) 192.
[6] G. Geoffroy, M.H. Mathon, A. Barbu, unpublished work.
[7] M. Akamatsu, PhD thesis, Paris XI-Orsay University, 1994.
[8] K. Farrell, R.E. Stoller, P. Jung, H. Ullmaier, J. Nucl. Mater. 279 (2000) 77.
[9] D.E. Alexander, L.E. Rehn, K. Farrell, R.E. Stoller, J. Nucl. Mater. 228 (1996) 68.
[10] L.K. Mansur, J. Nucl. Mater. 216 (1994) 97.
[11] N.M. Ghoniem, S. Sharafat, J. Nucl. Mater. 92 (1980) 121.
[12] A.C. Hindmarsh, LLNL Report UCRL-88007, 1982.
[13] O.S. Oen, Cross-sections for atomic displacements in solids by fast electrons, Report ORNL-4897, 1973.
[14] W.A. Coghlan, M.H. Yoo, in: Proceeding Conference on the Role of Dislocation Theory in Modelling Physical Systems, Florida, Pergamon, Oxford, 1980, p. 152.
[15] R. Bullough, D.W. Wells, J.R. Willis, M.H. Wood, Cross-sections for atomic displacements in solids by fast electrons, Report ORNL-4897, 1973, p. 116.
[16] W.G. Wolfer, M. Ashkin, J. Appl. Phys. 46 (2) (1975) 547.
[17] A. Si-Amhed, W.G. Wolfer, Cross-sections for atomic displacements in solids by fast electrons, Report ORNL-4897, 1973, p. 142.
[18] C.H. Woo, J. Nucl. Mater. 107 (1982) 20.
[19] R.E. Stoller, in: A.S. Kumar, D.S. Gelles, R.K. Nanstadt, E.A. Little (Eds.), ASTM STP 1175, American Society of Testing and Materials, Philadelphia, PA, 1993, p. 394.
[20] M.R. Hayns, J. Nucl. Mater. 56 (1975) 267.

[21] A. Seeger, U. Gösele, Phys. Lett. 61A (1977) 423.
[22] N. Soneda, T. Diaz de la Rubia, Philos. Mag. 78 (5) (1998) 995.
[23] J.P. Hirth, J. Lothe, Theory of Dislocations, 2nd Ed., Krieger, Malabar, FL, 1992.
[24] R. Bullough, M.R. Hayns, M.H. Wood, J. Nucl. Mater. 90 (1980) 44.
[25] A. Duong-Hardouin Duparc, PhD thesis, Paris XI-Orsay University, 1997.
[26] P. Moser, C. Corbel, P. Lucasson, P. Hautojarvi, Mater. Sci. Forum 15–18 (1987) 925.
[27] L. Brown, A. Kelly, R.M. Mayer, Philos. Mag. 19 (1969) 721.
[28] A. Bourret, Radiat. Eff. 5 (1977) 27.
[29] M.K. Hossain, L.M. Brown, Radiat. Eff. 31 (1977) 203.
[30] Landolt-Börnstein, Numerical Data and Functional Relationships in Science and Technology, vol. 25, Atomic Defects in Metals, Springer.
[31] R.A. Johnson, Phys. Rev. 134 (5A) (1964) A1329.
[32] R.E. Stoller, G.R. Odette, J. Nucl. Mater. 251 (1997) 49.
[33] R. Vascon, N.V. Doan, Radiat. Eff. Def. Solids 141 (1996) 375.
[34] C.S. Becquart, C. Domain, A. Legris, J.C. Van Duysen, J. Nucl. Mater. 280 (2000) 73.
[35] A.R. Alnatt, A.B. Lidiard, Atomic Transport in Solids, Cambridge University, Cambridge, 1993.